

Seismicity patterns of earthquake swarms due to fluid intrusion and stress triggering

Sebastian Hainzl*

Institute of Geosciences, University of Potsdam, Potsdam, Germany

Accepted 2004 August 24. Received 2004 August 4; in original form 2004 March 19

SUMMARY

Earthquake swarms are often assumed to result from an intrusion of fluids into the seismogenic zone, causing seismicity patterns which significantly differ from aftershock sequences. But neither the temporal evolution nor the energy release of earthquake swarms is generally well understood. Because of the lack of descriptive empirical laws, the comparison with model simulations is typically restricted to aspects of the overall behaviour such as the frequency–magnitude distribution. However, previous investigations into a large earthquake swarm which occurred in the year 2000 in Vogtland/northwest Bohemia, Central Europe, revealed some well-defined characteristics which allow a rigorous test of model assumptions. In this study, simulations are performed of a discretized fault plane embedded in a 3-D elastic half-space. Earthquakes are triggered by fluid intrusion as well as by co-seismic and post-seismic stress changes. The model is able to reproduce the main observations, such as the fractal temporal occurrence of earthquakes, embedded aftershock sequences, and a power-law increase of the average seismic moment release. All these characteristics are found to result from stress triggering, whereas fluid diffusion is manifested in the spatiotemporal spreading of the hypocentres.

Key words: fluids in rock, geostatistics, seismic modelling, seismic stress, seismicity, synthetic earthquake catalogues.

1 INTRODUCTION

The two most important types of earthquake clustering are aftershock sequences and earthquake swarms. Aftershocks are associated with a main shock and their rate of occurrence can be generally described by the modified Omori law, $\lambda \sim (c + t)^{-p}$, where t is the time elapsed since the main shock, p is close to 1 and c is a small time constant (Utsu *et al.* 1995). The spatial distribution of aftershocks is observed to correlate with the static stress-field changes of the main shock, suggesting that stress triggering plays an important role (Stein 1999). An additional mechanism is needed to explain the time delay of aftershocks, such as a rate-state friction law (Dieterich 1994), post-seismic relaxation (Savage & Svarc 1997; Hainzl *et al.* 1999), afterslip (Burgmann *et al.* 2002; Perfettini & Avouac 2004) or locally induced fluid flows (Nur & Booker 1972).

In contrast to aftershocks which accompany main shocks, earthquake swarms are not characterized by a dominant earthquake and their temporal evolution cannot be described by any simple law comparable to the Omori law. These clusters are often assumed to result from an intrusion of fluids reducing the resistance of faults (Kisslinger 1975; Noir *et al.* 1997; Yamashita 1999). Each earthquake within the swarm redistributes stress, which may in turn in-

fluence the subsequent swarm evolution, especially if the crust is in a critical state (Main 1996). Slider-block models have shown that earthquake swarms can result from a self-organized critical stress field without any external pore pressure source (Hainzl 2003). In general, the absence of well-defined swarm characteristics prevents the testing of different model assumptions. In this paper, we thus concentrate on a specific earthquake swarm which occurred in 2000 in Vogtland/northwest Bohemia, Central Europe. This region is well known for the episodic occurrence of earthquake clusters which consist of small-magnitude events. Preliminary results of isotope investigations suggest that the swarm activity in this region is induced by fluid overpressure (Weinlich *et al.* 1999; Brauer *et al.* 2003). This assumption is supported by the observation that fluid diffusion like spreading of the hypocentres occurred during the swarm activity (Parotidis *et al.* 2003). However, the earthquake swarm activity also shares some common features with tectonic earthquake clusters, in particular embedded aftershock sequences according to the Omori law which point to an important role for stress triggering (Hainzl & Fischer 2002). In addition to these observations, further characteristics of the Vogtland earthquake swarm can be used to test different model assumptions, including:

(1) whether the temporal occurrence of the earthquakes, which take place on approximately the same fault plane (Fischer 2003), is fractal (clustered on all time scales), in particular if the inter-event time distribution can be described by the power law $t^{-1.5}$; and

*Pacific Region Office, GJI.

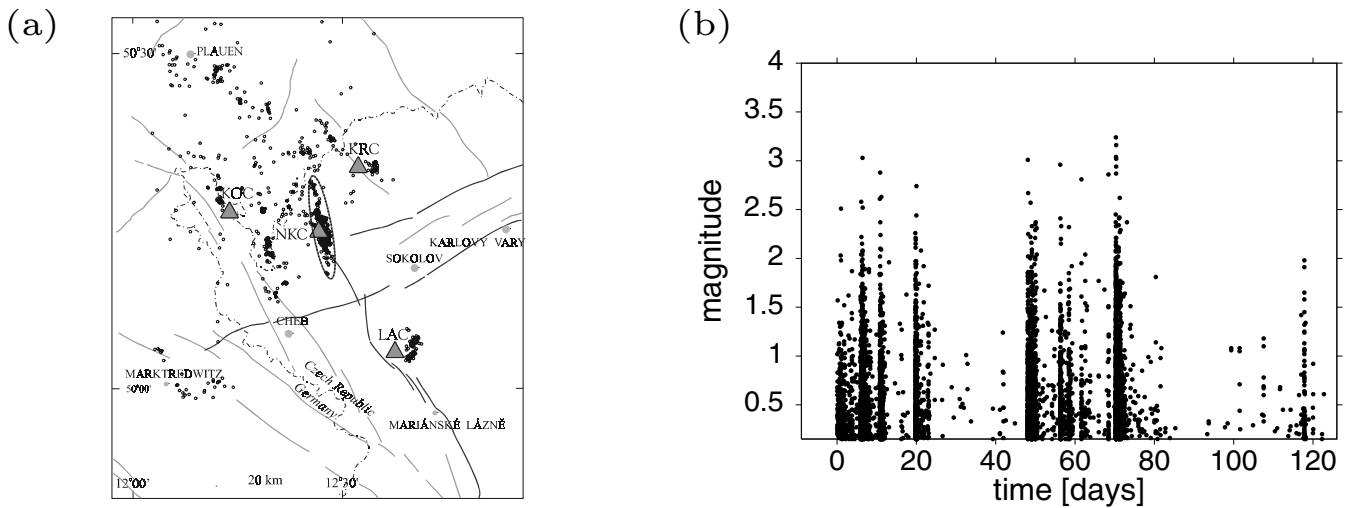


Figure 1. (a) The fault structure (line segments) of the Vogtland/northwest Bohemia earthquake swarm region and earthquake epicentres (circles). The main swarm area is marked by the ellipse enclosing the year 2000 swarm activity. (b) The local earthquake magnitudes of this swarm are shown as a function of time elapsed since 2000 August 28.

(2) whether the average seismic moment release has increased during the swarm evolution according to $\langle M_0 \rangle \propto i^{1/4}$, where i is the earthquake index (Hainzl & Fischer 2002).

The earthquake model which is investigated in this paper incorporates 3-D elastic stress interactions and pore pressure variations due to fluid intrusion (Section 2). It will be shown that a combination of changes in both stress and pore pressure explains the main characteristics of the Vogtland/northwest Bohemia earthquake swarm (Section 3).

2 MODEL

The analysed model is mostly similar to the model of Yamashita (1997, 1998), which was introduced to simulate seismicity patterns initiated by fluid migration in a narrow, porous, planar fault zone pre-stressed by tectonic plate movement or local deformation and embedded in a 3-D elastic half-space. Additionally, we assume post-seismic creep on the fracture zone which leads to realistic aftershock activity according to the Omori law. This new mechanism will be described in more detail in Section 2.1.

The model is adapted to the Vogtland earthquake swarm which occurred between August and December in the year 2000 in the Novy Kostel focal area. It is the most recent and best-documented strong earthquake swarm in Vogtland/northwest Bohemia (Fig. 1a). The earthquake catalogue of this swarm was recorded by the WEBNET local seismic network (Horalek *et al.* 2000) and consists of more than 8400 earthquakes with local magnitude $M_L \geq -0.5$ (Fischer 2003). The catalogue is found to be complete for the $N = 4823$ earthquakes with $M_L \geq 0.2$ (Hainzl & Fischer 2002). Fig. 1(b) shows the earthquakes of this swarm event as a function of their occurrence times.

The fault plane of the Vogtland earthquake swarm is modelled with a 3 km × 3 km rectangular patch dipping 73°. The lower edge of the brittle segment is set to a depth of 10 km (see Fig. 2a). The fault is discretized into 50 × 50 cells of dimension 60 m × 60 m each. Earthquake slip occurs when the Coulomb failure stress (CFS) becomes positive at one cell, i.e. the Coulomb failure criterion is fulfilled (Harris 1998):

$$CFS \equiv \tau - \mu(\sigma - P) \geq 0. \tag{1}$$

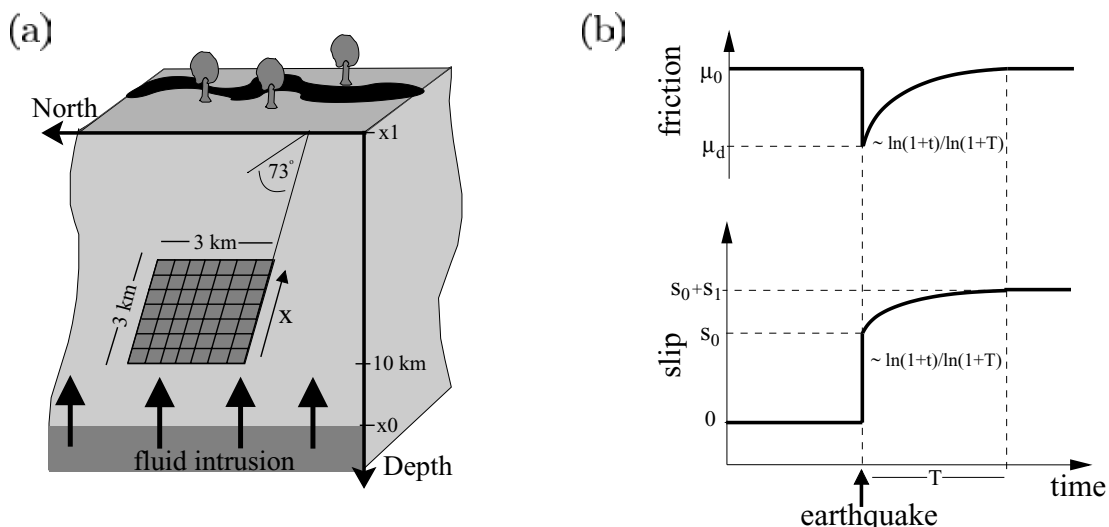


Figure 2. Illustration of the model configuration (a) and the assumed healing and slip characteristics (b).

Here τ defines the shear and σ the normal stress (positive for compression), P is the pore pressure and μ is the coefficient of friction. Earthquake slip on the fault affects neither the normal stress nor the mean stress on the fault plane. Thus, slip has no effect on the pore pressure if material properties (e.g. permeability) are constant. In contrast, fluid flow generally influences not only the pore pressure but also the stress field. However, because of the numerical costs that would be involved in modelling the full coupling, it is assumed here that the stress field is, to a first order, not influenced by fluid flow (pore pressure changes).

The characteristics of co-seismic slip are governed by a static/kinetic friction law (Ben-Zion & Rice 1993). If sliding is initiated, the coefficient of friction μ , i.e. the frictional resistance, drops from its static value μ_0 to its lower dynamic value μ_d and remains there until the earthquake is terminated. The dynamic weakening of the fault strength is accompanied by a drop in stress. The shear stress τ drops to the arrest stress τ_a which is smaller than the frictional dynamic stress $\mu_d(\sigma - p)$ because of dynamic overshoot.

The stress change on the fault plane due to relative slip of one segment is calculated with the analytical solution given by Okada (1992) for an elastic Poisson solid with a rigidity of 30 GPa. For simplification, we assume the slip to always be in the strike direction, although this is not in perfect agreement with the observed Vogtland swarm where both normal and strike-slip events occurred (Fischer 2003). However, the main characteristics of the model are expected to be independent of this restriction because the stress pattern on the fault changes only slightly for rotating slip on the same fault plane. In particular, the stress decreases inside the rupture zone in the same way, and increases everywhere else. This increase is only slightly larger in the direction of slip.

The sliding of one cell can lead to an instability in other cells, and so on. An earthquake ends when all cells are stable with regard to the Coulomb failure criterion (eq. 1). The duration of earthquakes is much shorter than the typical time separating subsequent earthquakes. Thus we assume instantaneous co-seismic slip, or, in other words, that the whole earthquake occurs at the same time.

2.1 Healing and post-seismic creep

To account for the healing characteristics observed in laboratory experiments after co-seismic slip (Dieterich 1972; Ruina 1983; Scholz 1998), the fault strength is assumed to recover according to

$$\mu(\Delta t) = \mu_d + (\mu_0 - \mu_d) \frac{\log(1 + \Delta t)}{\log(1 + T)}, \quad (2)$$

where T is the time interval required for complete healing and Δt is the time elapsed since the earthquake occurred (measured in minutes). An illustration of this characteristic is shown in Fig. 2(b).

It is known from laboratory experiments that logarithmic healing results from asperity creep on the fracture zone, which leads to an increase of the contact area (Scholz & Engelder 1976). In the model it is assumed that after co-seismic slip the dislocation slowly extends further as creep on the earthquake rupture area which adapts to the observed afterslip characteristics in a simplified way (Burgmann *et al.* 2002). It is straightforward to assume that the afterslip is correlated with strength; that is, slip increases logarithmically according to

$$s(\Delta t) = s_0 + s_1 \frac{\log(1 + \Delta t)}{\log(1 + T)}, \quad (3)$$

where s_0 and s_1 refer to the co-seismic and post-seismic slip. The fraction of post-seismic slip $\kappa \equiv s_1/(s_0 + s_1)$ is a model parameter.

The slip characteristic is illustrated in the lower part of Fig. 2(b). The stress changes due to afterslip are again calculated with the analytical solution given by Okada (1992).

2.2 Fluid diffusion

It has been previously shown (Shapiro *et al.* 1997; Yamashita 1997) that variations in pore pressure in the fault plane which result from an intrusion of fluids from a high-pressure source can be described by the diffusion equation

$$\frac{\delta}{\delta t} P = D \frac{\delta^2}{\delta x^2} P, \quad (4)$$

where D is the hydraulic diffusivity which is generally expected to be between 0.01 and 10 m² s⁻¹ in the crust (Scholz 2002).

Neglecting more sophisticated mechanisms such as pore creation (Yamashita 1999), homogeneous and constant hydraulic conditions are assumed. The diffusivity within the fault zone is set to the empirically estimated value in the Vogtland region, $D = 0.27$ m² s⁻¹ (Parotidis *et al.* 2003), whereas the permeability of the host rock is assumed to be negligible. Furthermore, pore pressure is initially constant on the fault plane. Then, a high-pressure source starts to release fluids at depth. The source is assumed to be laterally extensive, thus the one-dimensional version of eq. (4) can be solved to find the deviations from the initial state. Furthermore, it is assumed that the fluid reservoir is large enough for the pressure to remain approximately constant at the source. The equation is solved in the range between the horizontal lines x_0 and x_1 on the fault plane, where x increases upwards and x_0 and x_1 mark the injection line and the surface, respectively (see Fig. 2a). We use the following boundary conditions: $P(x_0, t) = \Delta P$, $P(x_1, t) = 0$, and $P(x, t = 0) = 0$ for $x > x_0$.

3 NUMERICAL SIMULATIONS

The evolution of slip and strength as well as the pore pressure diffusion are simulated by means of a finite difference scheme with a time step of 10 s. The initial stress values $\tau(t = 0)$ are distributed within the arrest stress τ_a and failure stress $\tau_f = \mu_0(\sigma - P(0))$ according to a doubly truncated Gaussian distribution, where the modal value of this distribution is fixed to the lower limit τ_a . The standard deviation is varied in order to study the influence of the pre-stress level ($\tau = (\tau - \tau_a)/(\tau_f - \tau_a)$). The normal stress σ , the pore pressure P and the static coefficient of friction μ are initially constant on the fault plane. The initial friction coefficient $\mu_0 \equiv \mu(t = 0)$ is set to 0.6 and the effective normal stress $\sigma - P(0)$ is arbitrarily set to 25 MPa. To account for heterogeneities of the brittle properties, the arrest stresses τ_a are uniformly distributed in the interval between 2 and 8 MPa; and the dynamic coefficient of friction varies between $\tau_a/25$ MPa and 0.6. An overview of all model parameters is given in Table 1.

Simulations are performed with different combinations of the free model parameters: (1) the stress level $\langle \tau \rangle$; (2) the depth of the fluid source x_0 ; (3) the increase in pore pressure ΔP ; (4) the healing time T ; and (5) the fraction of post-seismic creep κ .

3.1 Results

The simulated seismicity is in very good agreement with the natural swarm occurrence in Vogtland. The main results are discussed for an example model simulation with parameters $\langle \tau \rangle = 0.4$, $x_0 = 10$ km, $\Delta P = 2$ MPa, $\kappa = 0.3$ and $T = 0.1$ d.

Table 1. Overview of model parameters.

Stage of cycle	Symbol	Value	Description
Pre-stress	$\langle \tau \rangle$	Free	Initial stress level
Fluid diffusion	x_0	Free	Depth of the source
	ΔP	Free	Increase in pore pressure at x_0
	D	$0.27 \text{ m}^2 \text{ s}^{-1}$	Hydraulic diffusivity in the fault zone
Co-seismic slip	μ_0	0.6	Static friction
	μ_d	0.08–0.6	Dynamic friction
	$\sigma - P(0)$	25 MPa	Initial effective normal stress
	τ_a	2–8 MPa	Arrest stress
Healing	T	Free	Healing time
Post-seismic slip	κ	Free	Ratio of post-seismic and total slip

3.2 Frequency–magnitude distribution

To show that the frequency–magnitude distribution can be fitted by a Gutenberg–Richter law, for each event we calculate a local magnitude M_L from its seismic moment M_0 (in N m) by means of the empirical relation for the Vogtland region, $M_L = 0.95 \log(M_0) - 10.76$ (Hainzl & Fischer 2002). The shape of the resulting frequency–magnitude distribution (Fig. 3c) is very similar to that of the Vogtland swarm earthquakes; the b value in particular is the same. Note that the shift between both distributions by a magnitude of about 0.2 could indicate a slightly modified relation, namely $M_L = 0.95 \log(M_0) - 10.56$.

3.3 Temporal occurrence

The earthquake activity is not dominated by one large event, instead it occurs in several subclusters separated in space and time

(Fig. 3a). In particular, the temporal occurrence of earthquakes is fractal, where the inter-event time distribution reproduces the empirically observed power law $\sim t^{-1.5}$ (Fig. 3b).

The subclusters themselves are very similar to typical aftershock sequences. To illustrate this, we examine the activity relative to the largest earthquakes within the swarm period. All earthquakes with local magnitude larger than 2.0 are considered as main shocks if they are the largest event within ± 2 hr. The activity accompanying the main shocks is formed by stacking the records relative to the main-shock occurrence times. The main shocks themselves are not counted. For comparison, the same analysis is performed for the Vogtland/northwest Bohemia earthquake swarm, where the same lower-magnitude cut-off ($M_{\text{cut}} = 0.8$) is used as in the model simulations. Fig. 4 shows the averaged foreshock and aftershock activity accompanying the 25 (34) main shocks with $M \geq 2$ within the simulation (Vogtland swarm). The curves reveal a very good agreement between simulation and observation regarding the level of activity

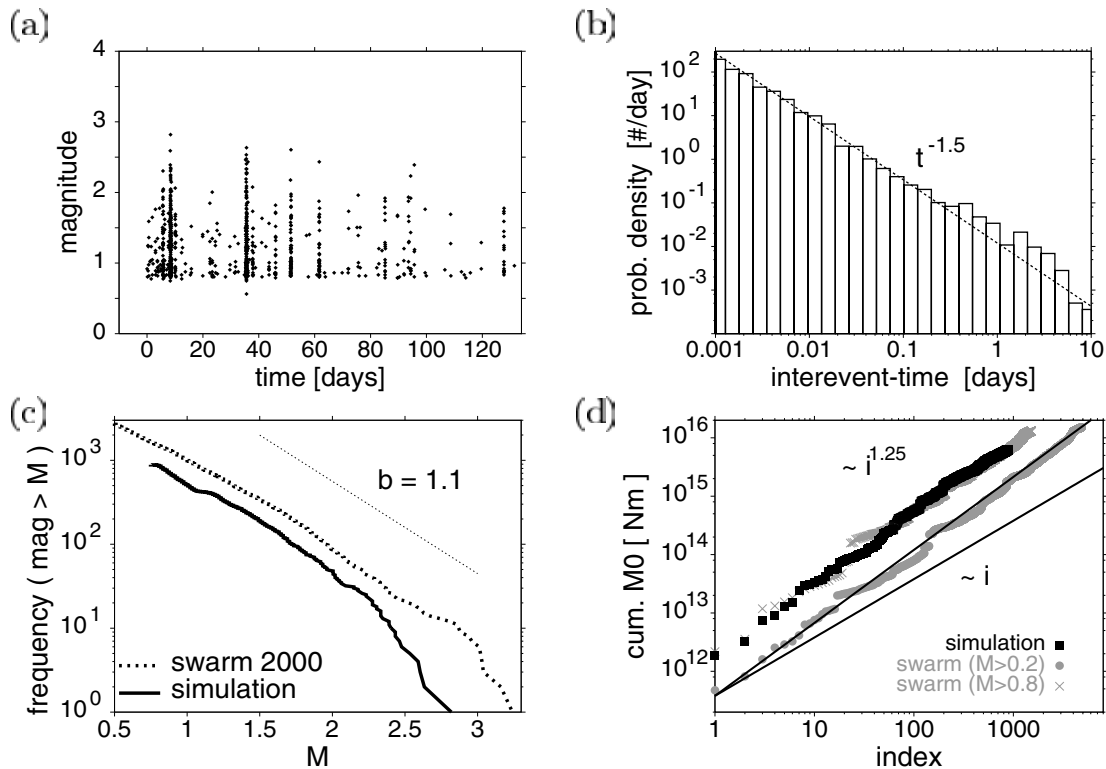


Figure 3. Example of a model simulation: (a) the magnitudes as a function of time; (b) the inter-event time–probability distribution; (c) the frequency–magnitude distribution; and (d) the cumulative seismic moment release as a function of the earthquake index i .

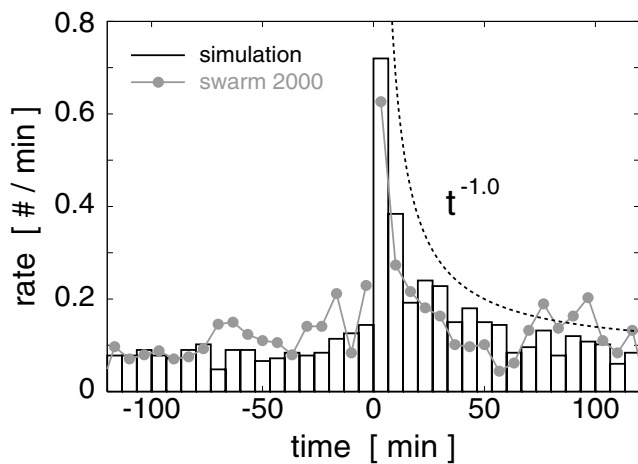


Figure 4. The stacked and averaged seismic rate relative to main shocks with $M_L \geq 2$ for the simulation in Fig. 3 (boxes) and the Vogtland earthquake swarm (solid curve). The aftershock decay is compared with the Omori law (dashed curve).

and the temporal evolution. Furthermore, the results are very similar to that expected for tectonic main shocks: the probability of aftershocks decays according to the Omori law (Utsu *et al.* 1995), and the number of aftershocks significantly exceeds the number of foreshocks.

3.4 Increasing seismic moments

Fig. 3(d) shows that the average seismic moment released per event increases monotonically during the evolution of the earthquake

swarm according to $M_0 \sim i^{0.25}$, where i is the earthquake index. Equivalently, the cumulative seismic moment release increases as $\sum M_0 \sim i^{1.25}$. Exactly the same relation has been found for the Vogtland earthquake swarm (Hainzl & Fischer 2002).

Note that a possible theoretical explanation of this relation can be derived from basic fracture mechanics, where it is known that stress at a crack tip scales with the crack extension c according to $\tau \sim \sqrt{c}$ (Scholz 2002). A crack model can be considered as a first-order approximation in the case in which earthquakes mainly occur at the edge of the previously ruptured zone. Then, stress successively accumulates at the tip of the growing rupture area. Assuming that each earthquake, on average, extends the cracked area A by the same amount, the crack extension scales with $c \sim \sqrt{A} \sim \sqrt{i}$ which leads to $\tau \sim i^{0.25}$. If the stress drop is proportional to the stress level, the empirically observed relation between seismic moment and earthquake number is explainable.

3.5 Spatiotemporal migration

Event hypocentres migrate during the simulated swarm evolution. As a result of fluid intrusion, activity starts at depth and spreads upwards with time. The extension of the rupture zone can be approximated by the theoretical curve, $\sqrt{4\pi Dt}$, describing the distance of the pressure front from the fluid source (Shapiro *et al.* 1997). This is illustrated in Fig. 5, where the hypocentral distance from the source is plotted as a function of the earthquake occurrence time for two case: the example of Figs 3 and 4 and an example with larger pore pressure increase but no afterslip, $\Delta P = 5$ MPa and $\kappa = 0$. In the latter case, only static stress changes are considered. Although the clustering characteristics are very different, a clear

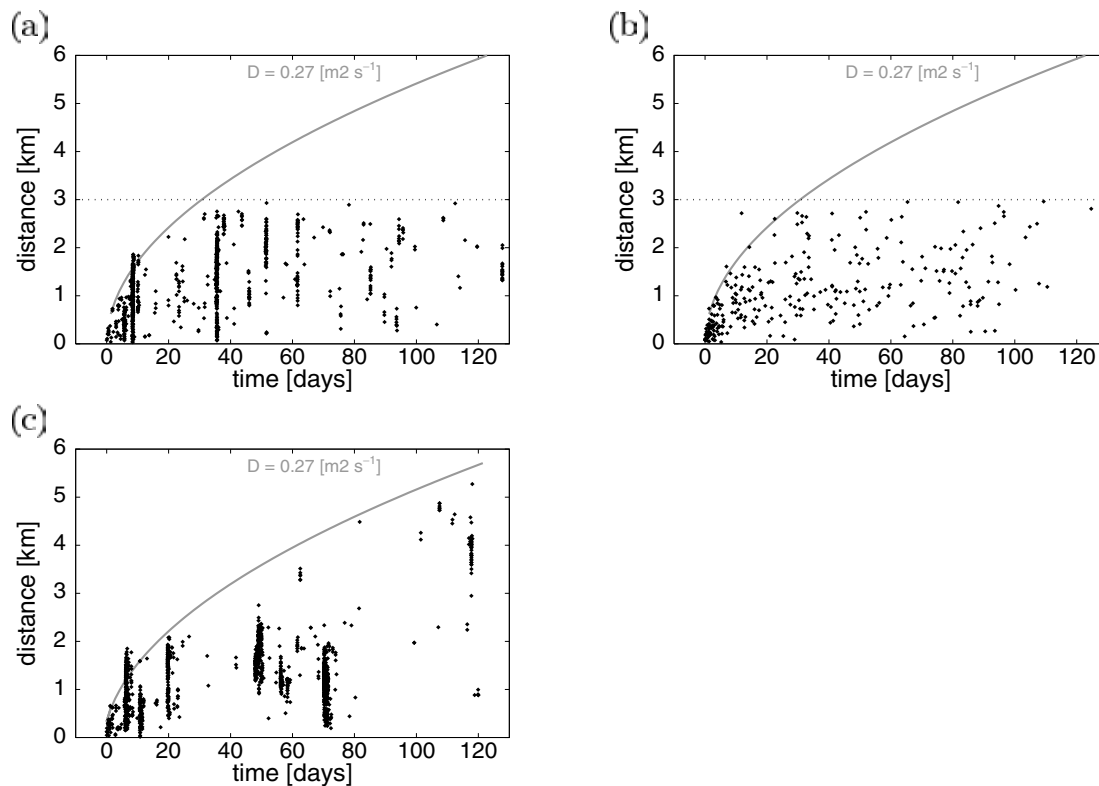


Figure 5. Distance of the hypocentre from the fluid source as a function of the earthquake occurrence times (a) for a simulation with ($\kappa = 0.3$) and (b) without post-seismic slip ($\kappa = 0$). The former simulation is that of Fig. 3. The dotted line refers in both plots to the system size which cannot be exceeded. (c) The corresponding plot for the Vogtland earthquakes with $M_L \geq 0.8$, where the fluid source is identified with the hypocentre of the first earthquake.

hypocentre migration is observed in both cases, where the majority of events occur within the parabolic envelope as theoretically expected. This observation reflects the fact that the initial stress state is subcritical; in other words an initial increase in the pore pressure is necessary to bring the fault into a critical state. The parabola marks the extension of the critical region as a function of time. Within the critical loaded region, the stress transfer due to the earthquakes (stress triggering) becomes the dominant triggering process leading to earthquake clustering.

3.6 Dependence on model parameters

In order to explore the parameter space of this model, simulations have been performed with different sets of model parameters $\langle\tau\rangle$, x_0 , ΔP , T and κ . In addition, simulations with a diffusivity D differing from the previously proposed value for Vogtland, $D = 0.27 \text{ m}^2 \text{ s}^{-1}$ have been investigated.

The initial stress level $\langle\tau\rangle$ determines whether the fault segment is in a subcritical, critical or supercritical state. Similar to the results found for slider-block models (Hainzl & Zöller 2001), earthquake ruptures cannot be stopped after growing beyond a critical size in overstressed (supercritical) faults. Thus for $\langle\tau\rangle \geq \langle\tau\rangle_{\text{crit}}$, the earthquake sequence rupturing the fault segment consists of a single dominant earthquake. On the other hand, if the stress level is too low, fluid diffusion takes place without seismicity. Swarm-like activity occurs for $\langle\tau\rangle < \langle\tau\rangle_{\text{crit}}$ if the pore pressure increase ΔP is sufficient to bring the fault close to the critical state. However, if the fault is initially in a critical state, an earthquake swarm can also spontaneously occur in the absence of pore pressure changes, $\Delta P = 0$, though swarm activity typically consists of only one cluster. In this case, earthquakes are triggered solely by afterslip and the afterslip rate decreases rapidly with time, thus the probability for a second subcluster separated in time becomes very small for $\Delta P = 0$, and the reproduction of the empirical observation of several subclusters is even more improbable.

We find that the post-seismic creep κ influences the number of directly triggered aftershocks. Thus κ is responsible for subclustering within the earthquake sequence, whereas the healing time T determines the duration of those subclusters. This is illustrated in Fig. 6(a), where the cumulative number of earthquakes is shown as a function of time in the case of three simulations differing in their κ value. The temporal occurrence is almost homogeneous and the resulting curve is smooth in the case of negligible afterslip ($\kappa = 0$). For increasing values of κ , the activity begins to cluster

in time. As a consequence, the inter-event time distribution changes from an exponential ($\kappa = 0$) to a fractal shape (see Fig. 6b).

The strength of the pore pressure increase ΔP has an effect on the total amount of seismicity. For small values of ΔP only a fraction of the fault plane ruptures. For larger values of ΔP the whole fault successively ruptures and multiple ruptures can occur at the same place. Furthermore, a variation of the depth of the fluid source x_0 slightly affects the overall seismicity pattern. In the case that the fluid source directly borders on the brittle fault region, the change in pore pressure is strongest in the initiation phase and decreases monotonically afterwards. For greater source depths, the rate of change of pore pressure increases in the beginning and consequently the seismic rate accelerates in the initiation phase.

The hydraulic diffusivity D mainly changes the spatiotemporal migration of activity. For smaller D , the intervals between subclusters become longer and the overall duration of the activity increases. Thus the hydraulic diffusivity influences the speed of the evolution of seismic activity.

In spite of these variabilities, the statistical features shown in Fig. 3 are robust for a large range of the model parameters $\langle\tau\rangle$, x_0 , ΔP , T , κ and D .

4 SUMMARY AND CONCLUSIONS

The well-defined characteristics of the earthquake swarm which occurred in 2000 in Vogtland/northwest Bohemia allow a detailed comparison with model simulations. We have analysed an earthquake model consisting of two mechanisms: fluid diffusion and stress triggering. The combination of both mechanisms is found to reproduce:

- (1) the frequency–size distribution with a b value close to 1;
- (2) self-similar clustering in time, especially the inter-event time distribution $\sim t^{-1.5}$;
- (3) embedded aftershock sequences according to the Omori law;
- (4) the increase of the average seismic moment per event $\sim t^{0.25}$; and
- (5) the spatiotemporal hypocentre migration approximately bounded by the theoretical curve $r = \sqrt{4\pi Dt}$.

Fluid diffusion is only reflected in the last characteristic, spatiotemporal hypocentre migration, although it is the primary triggering mechanism for the activity in general. However, after the fault patch has been brought into a critical state by an increase in pore pressure, stress triggering becomes dominant. The post-seismic stress changes due to afterslip are particularly important for the

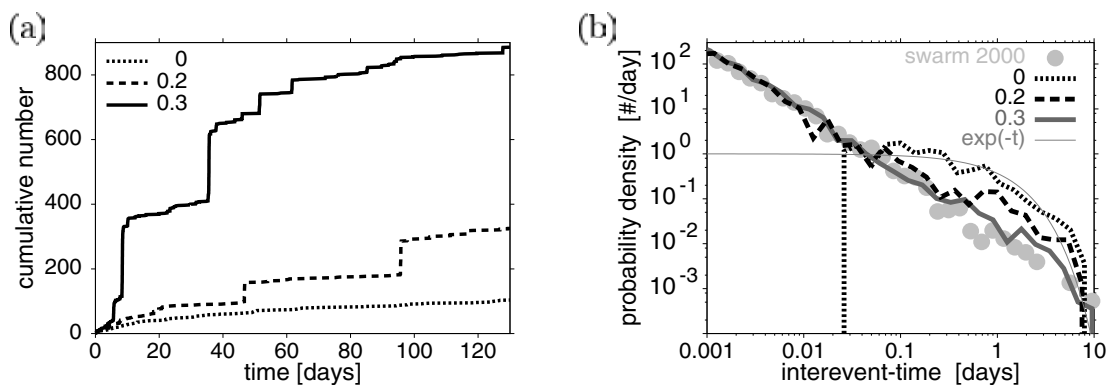


Figure 6. (a) The number of earthquakes as a function of the swarm duration for three simulations (depth of the fluid source $x_0 = 10 \text{ km}$, increase in pore pressure $\Delta P = 2 \text{ MPa}$, and healing time $T = 0.1 \text{ d}$) with different values of fraction of post-seismic creep $\kappa = 0, 0.2$ and 0.3 . For the same examples, (b) shows the inter-event time–probability distribution in comparison with that observed for the Vogtland swarm earthquakes with $M_L \geq 0.8$.

characteristics of short-term clustering. Thus the mechanism of afterslip is in good agreement with empirical observations. However, the reproduction of the empirical laws does not necessarily imply a validation of the assumed mechanisms. Afterslip is one of only several possible mechanisms for aftershocks, and has been chosen because of its low computational costs which allow extended simulations. It remains an open question whether other mechanisms, such as a rate- and state-dependent friction (Dieterich 1994) or stress corrosion cracking (Shaw 1993; Main 2000), are also able to reproduce the observations.

In summary, model simulations indicate that the Vogtland earthquake swarm was initially triggered by a diffusion-like increase in pore pressure. The most striking characteristics of this swarm, however, can be explained by earthquake-induced stress changes causing a pronounced earthquake clustering and accelerated seismic moment release.

ACKNOWLEDGMENTS

The author wishes to thank John Beavan, Russell Robinson and an anonymous reviewer for valuable suggestions. Tomas Fischer and Lindsay Schoenbohm are thanked for stimulating discussions and discerning reading of the manuscript. This work was supported by the Deutsche Forschungsgemeinschaft (SCH280/13-2).

REFERENCES

- Ben-Zion, Y. & Rice, J.R., 1993. Earthquake failure sequences along a cellular fault zone in a three-dimensional elastic solid containing asperity and nonasperity regions, *J. geophys. Res.*, **98**, 14 109–14 131.
- Brauer K., Kampf, H., Strauch, G. & Weise, S.M., 2003. Isotopic evidence (He-3/He-4, C-13(CO₂)) of fluid-triggered intraplate seismicity, *J. geophys. Res.*, **108**, 2070, doi:10.1029/2002JB002077.
- Burgmann, R., Ergintav, S., Segall, P., Hearn, E. H., McClusky, S., Reilinger, R.E., Woith, H. & Zschau, J., 2002. Time-dependent distributed afterslip on and deep below the Izmit earthquake rupture, *Bull. seism. Soc. Am.*, **92**, 126–137.
- Dieterich, J.H., 1972. Time-dependent friction in rocks, *J. geophys. Res.*, **77**, 3690–3697.
- Dieterich, J.H., 1994. A constitutive law for rate of earthquake production and its application to earthquake clustering, *J. geophys. Res.*, **99**, 2601–2618.
- Fischer, T., 2003. The August–December 2000 earthquake swarm in NW Bohemia: the first results based on automatic processing of seismograms, *J. Geodyn.*, **35**, 59–81.
- Hainzl, S., 2003. Self-organization of earthquake swarms, *J. Geodyn.*, **35**, 157–172.
- Hainzl, S. & Fischer, T., 2002. Indications for a successively triggered rupture growth underlying the 2000 earthquake swarm in Vogtland/NW Bohemia, *J. geophys. Res.*, **107**, 2338, doi:10.1029/2002JB001865.
- Hainzl, S. & Zöller, G., 2001. The role of disorder and stress concentration in nonconservative fault systems, *Physica A*, **294**, 67–84.
- Hainzl, S., Zöller, G. & Kurths, J., 1999. Similar power laws for foreshock and aftershock sequences in a spring-block model for earthquakes, *J. geophys. Res.*, **104**, 7243–7254.
- Harris, R., 1998. Introduction to special section: stress triggers, stress shadows, and implications for seismic hazard, *J. geophys. Res.*, **103**, 24 347–24 358.
- Horalek, J., Fischer, T., Bouskova, A. & Jedlicka, P., 2000. Western Bohemia/Vogtland in the light of the WEBNET network, *Stud. Geophys. Geod.*, **44**, 107–125.
- Kisslinger, C., 1975. Processes during the Matsushiro swarm as revealed by leveling, gravity, and spring–flow observations, *Geology*, **3**, 57–62.
- Main, I.G., 1996. Statistical physics, seismogenesis, and seismic hazard, *Rev. Geophys.*, **34**, 433–462.
- Main, I.G., 2000. A damage mechanics model for power-law creep and earthquake aftershock and foreshock sequences, *Geophys. J. Int.*, **142**, 151–161.
- Noir, J., Jacques, E., Bekri, S., Adler, P.M., Taponnier, P. & King, G.C.P., 1997. Fluid flow triggered migration of events in the 1989 Dobi earthquake sequence of Central Afar, *Geophys. Res. Lett.*, **24**, 2335–2338.
- Nur, A. & Booker, J.R., 1972. Aftershocks caused by pore fluid flow?, *Science*, **175**, 885–887.
- Okada, Y., 1992. Internal deformation due to shear and tensile faults in a half-space, *Bull. seism. Soc. Am.*, **82**, 1018–1040.
- Parotidis, M., Rothert, E. & Shapiro, S.A., 2003. Pore-pressure diffusion: a possible triggering mechanism for the earthquake swarms 2000 in Vogtland/NW-Bohemia, central Europe, *Geophys. Res. Lett.*, **30**, 2075, doi:10.1029/2003GL018110.
- Perfettini, H. & Avouac, J.-P., 2004. Postseismic relaxation driven by brittle creep: a possible mechanism to reconcile measurements and the decay rate of aftershocks, application to the Chi-Chi earthquake, Taiwan, *J. geophys. Res.*, **109**, B02304, doi:10.1029/2003JB002488.
- Ruina, A.L., 1983. Slip instability and state variable friction laws, *J. geophys. Res.*, **88**, 10 359–10 370.
- Savage, J.C. & Svarc, J.L., 1997. Postseismic deformation associated with the 1992 $M_w = 7.3$ Landers earthquake, southern California, *J. geophys. Res.*, **102**, 7565–7577.
- Scholz, C.H., 1998. Earthquakes and friction laws, *Nature*, **391**, 37–42.
- Scholz, C.H., 2002. *The Mechanics of Earthquakes and Faulting*, Cambridge University Press, Cambridge.
- Scholz, C.H. & Engelder, T., 1976. Role of asperity indentation and ploughing in rock friction, *Int. J. Rock Mech. Min. Sci.*, **13**, 149–154.
- Shapiro, S.A., Huenges, E. & Borm, G., 1997. Estimating the crust permeability from fluid-injection-induced seismic emission at the KTB site, *Geophys. J. Int.*, **131**, F15–F18.
- Shaw, B.E., 1993. Generalized Omori law for aftershocks and foreshocks from a simple dynamics, *Geophys. Res. Lett.*, **20**, 907–910.
- Stein, R.S., 1999. The role of stress transfer in earthquake occurrence, *Nature*, **402**, 605–609.
- Utsu, T., Ogata, Y. & Matsu'ura, R.S., 1995. The centenary of the Omori formula for a decay law of aftershock activity, *J. Phys. Earth*, **43**, 1–33.
- Weinlich, F.H., Brauer, K., Kampf, H., Strauch, G., Tesar, J. & Weise, S.M., 1999. An active subcontinental mantle volatile system in the western Eger rift, Central Europe: gas flux, isotopic (He, C, N) and compositional fingerprints, *Geochim. Cosmochim. Acta*, **63**, 3653–3671.
- Yamashita, T., 1997. Mechanical effect of fluid migration on the complexity of seismicity, *J. geophys. Res.*, **102**, 17 797–17 806.
- Yamashita, T., 1998. Simulation of seismicity due to fluid migration in a fault zone, *Geophys. J. Int.*, **132**, 674–686.
- Yamashita, T., 1999. Pore creation due to fault slip in a fluid-permeated fault zone and its effect on seismicity: generation mechanism of earthquake swarm, *Pageoph*, **155**, 625–647.